

Accepted Manuscript

Mechanical behavior of biopolymer composite coatings on plastic films by depth-sensing indentation – A nanoscale study

Cesare Rovera, Carlo A. Cozzolino, Masoud Ghaani, Davide Morrone, Richard T. Olsson, Stefano Farris

PII: S0021-9797(17)31278-X
DOI: <https://doi.org/10.1016/j.jcis.2017.10.108>
Reference: YJCIS 22978

To appear in: *Journal of Colloid and Interface Science*

Received Date: 5 July 2017
Revised Date: 24 October 2017
Accepted Date: 29 October 2017

Please cite this article as: C. Rovera, C.A. Cozzolino, M. Ghaani, D. Morrone, R.T. Olsson, S. Farris, Mechanical behavior of biopolymer composite coatings on plastic films by depth-sensing indentation – A nanoscale study, *Journal of Colloid and Interface Science* (2017), doi: <https://doi.org/10.1016/j.jcis.2017.10.108>

This is a PDF file of an unedited manuscript that has been accepted for publication. As a service to our customers we are providing this early version of the manuscript. The manuscript will undergo copyediting, typesetting, and review of the resulting proof before it is published in its final form. Please note that during the production process errors may be discovered which could affect the content, and all legal disclaimers that apply to the journal pertain.



Mechanical behavior of biopolymer composite coatings on plastic films by depth-sensing indentation – A nanoscale study

Cesare Rovera,^a Carlo A. Cozzolino,^a Masoud Ghaani,^a Davide Morrone,^{b,c} Richard T. Olsson,^d Stefano Farris^{a,e,}*

^a DeFENS, Department of Food, Environmental and Nutritional Sciences—Packaging Division, University of Milan, via Celoria 2 – 20133 Milan, Italy

^b R&D srl Tecnologie dei Materiali, Galleria Gandhi, 2 – 20017 Mazzo di Rho, Italy

^c Nanovea Inc., 6 Morgan, Ste 156, Irvine, CA – 92618, USA

^d Department of Fibre and Polymer Technology, School of Chemical Science and Engineering, KTH Royal Institute of Technology, Teknikringen 56, SE-100 44 Stockholm, Sweden

^e INSTM, National Consortium of Materials Science and Technology, Local Unit University of Milan, via Celoria 2 – 20133 Milan, Italy

*Corresponding author. Tel.: +39 0250316654; Fax: +39 0250316672

E-mail address: stefano.farris@unimi.it (S. Farris)

ABSTRACT. Fundamental physical behaviors of materials at the nanoscale level are crucial when local aspects govern the macroscale performance of nanocomposites, e.g., interface and surface phenomena. Because of the increasing interest in biopolymer nanocomposite coatings for many different applications (e.g., optical devices, displays/screens, and packaging), this work investigates the potential of nanoindentation as a method for clarifying the interplay between distinct phases (i.e., organic and inorganic) at local level in thin biopolymer films loaded with nanoparticles. The nanomechanical features of pullulan nanocomposite coatings laid on polyethylene terephthalate (PET) were quantified in terms of elastic modulus (E), hardness (H), and creep (C) through an instrumented indentation test composed of a loading-holding-unloading cycle. Colloidal silica (CS) and cellulose nanocrystals (CNCs) were used as spherical and rod-like nanoparticles, respectively. An overall reinforcing effect was shown for all nanocomposite coatings over the pristine (unfilled) pullulan coating. A size effect was also disclosed for the CS-loaded surfaces, with the highest E value recorded for the largest particles (8.19 ± 0.35 GPa) and the highest H value belonging to the smallest ones (395.41 ± 25.22 MPa). Comparing CS and CNCs, the addition of spherical nanoparticles had a greater effect on the surface hardness than cellulose nanowhiskers (353.50 ± 83.52 MPa and 321.36 ± 43.26 MPa, respectively). As for the elastic modulus, the addition of CS did not provide any improvement over both the bare and CNC-loaded pullulan coatings, whereas the coating including CNCs exhibited higher E values ($p < 0.05$). Finally, CS-loaded pullulan coatings were the best performing in terms of C properties, with an average indentation depth of 16.5 ± 1.85 nm under a load of ~ 190 μ N. These results are discussed in terms of local distribution gradients, surface chemistry of nanoparticles, and how nanoparticle aggregation occurred in the dry nanocomposite coatings.

KEYWORDS: *aggregation; biopolymer; cellulose nanocrystals (CNCs); coating; interface; nanoindentation; nanocomposite; phase separation; pullulan; surface*

ACCEPTED MANUSCRIPT

1. Introduction

The progress in indentation testing over the past thirty years has allowed indentation to be routinely performed on “nano” scales [1]. Nanoindentation, also referred to as “depth-sensing indentation” (DSI), is nowadays a widely applied technique for the measurement of the mechanical properties and behavior of material surfaces in the nanoscale range. After metals and ceramics, the application of instrumented indentation techniques to nontraditional materials such as polymers and biological materials has rapidly increased in the last decade [2]. Hardness and elastic modulus are the main properties derived from a nanoindentation experiment. However, a variety of additional physico-mechanical information can be gathered, including creep parameters, fracture toughness, and residual stresses [3]. Recent progress in instrument engineering has made it possible to achieve unprecedented performance in current apparatuses, overcoming previous bottlenecks, such as time-consuming experiments and extensive calibration procedures [4]. For this reason, nanoindentation now finds wide application not only in academia and research laboratories but also for quality control in mass production industries, such as semiconductors, aerospace, micro electro-mechanical systems (MEMS), monitors, optoelectronics, and, more recently, biological materials and food products [3].

The most attractive feature of nanoindentation is its capability to provide detailed information from a high local deformation (most used indenter tips have an area of approximately $0.0032 \mu\text{m}^2$) [5], which is of great importance for systems with limited dimensionality, e.g., thin films and coatings [6]. With the continuously emerging nanotechnologies in polymer manufacturing and processing, nanoindentation has also become a necessary tool for the characterization of nanostructured and nanocomposite polymeric materials. Not only does nanoindentation permit identification of transition zones between phases in heterogeneous materials, but it has also been proven to be a valuable technique to investigate filler content and size [7], filler dispersion [8], and, in particular, adhesion at the nanofiller-polymer matrix interface at very low sensitivity ranges [9].

Moreover, the interest in the synthesis of biomimetic materials (e.g., synthetic skins [10], artificial cell systems [11], and nanotextured implants [12] and functional particles [13]) has demonstrated nanoindentation as the ideal method for probing local gradients and heterogeneities in natural materials and for examining their hierarchical and multiscale organization. Nanoindentation can therefore be expected to be a very useful method in the evolving field of bio-based polymer nanocomposite systems that serve to replace oil-based polymers with polymers partially or totally obtained from renewable resources because these systems often exhibit novel unexplored material interactions at the surface of the nanophase. Within the field of biopolymer-based systems, the development of biocomposite thin films and coatings incorporating nanobuilding blocks (NBBs) has dramatically increased in recent years. In particular, the deposition of high-performance bionanocomposite coatings on plastic films is emerging in different fields (e.g., optical devices, displays and screens, and food packaging) to achieve extra benefits over conventional fillers while fulfilling recent trends toward “green” strategies [14,15]. In these systems, the properties of the nanocomposite layer depend largely on the interaction between the matrix and the filler [16]. Lack of affinity at the interface between the two phases (biopolymer network and nanofiller) can possibly arise for a number of reasons, such as chemical heterogeneity, thermodynamic incompatibility, physical hindrance, molecular arrangements, etc. These can eventually lead to diverse undesirable phenomena, e.g., interfacial de-bonding, phase segregation, filler aggregation/re-agglomeration, and increase in void content, which may in turn dramatically affect the material’s performance in terms of permeability of gases and vapors (increase in the diffusion coefficient) [17], mechanical integrity (crack formation and propagation) [18], optical properties (scattering centers) [19], dielectric performance (charge accumulation) [20], and thermal stability [21]. Therefore, the design of nanocomposite coatings would benefit from a fast and robust technique that enables the quantitative description of the mechanical performance on a nanoscale. However, to achieve this goal, it is crucial to prevent any potential influence of the supporting substrate, which might happen especially when thin and soft matters (e.g., most biopolymer coatings) with viscoelastic behavior

are deposited on stiffer substrates, such as plastic films. Making sure to obtain reliable information uniquely related to the coating alone in nanoindentation experiments is thus indispensable to avoid misleading results and misinterpretation of the coatings' performance.

In this work, we report for the first time on nanoindentation experiments on biopolymer nanocomposite coatings on a plastic film in an attempt to quantitatively assess the suitability of this technique for this special case of double-layered systems (i.e., flexible plastic substrate and thin biopolymer nanocomposite coating). More specifically, pullulan was used as a biopolymer phase due to its striking features in terms of high flexibility and optical properties, which are due to its fully amorphous organization [22,23]. Because of its uncharged nature, pullulan is able to interact with polar counterparts (e.g., particles, polymers, etc.) bearing a positive, negative, or neutral charge through ion-dipole and dipole-dipole (e.g., hydrogen bond) interactions. In addition, pullulan aqueous solutions are stable over a broad range of pH, thus expanding the possibility to use this biopolymer in different media. Colloidal silica (CS) and cellulose nanocrystals (CNCs) were used as representative spherical and rod-like NBBs, respectively. Both particles find widespread use for many different applications as nanoscale reinforcing fillers [24,25]. CS is used in papermaking, packaging, construction, electronics, photography, metal casting, and in the production of paints, beverages, and polishes [26], especially due to its optical (transparency and refractive index), mechanical (scratch resistance), and thermal properties [27]. For example, addition of the silica nanoparticle to the low- k organic thermosets has been demonstrated to enhance both the modulus and the hardness while reducing the coefficient of thermal expansion of the resultant transparent nanocomposite thin films [28]. Since the last decade, the interest in CNCs has dramatically increased for a number of applications relevant to the fields of material science and biomedical engineering due to its renewable nature, anisotropic shape, remarkable mechanical properties, good biocompatibility, tailorable surface chemistry, and excellent optical properties [29]. CNCs have been used to obtain transparent films, flexible displays, biomedical implants, fibers and textiles, separation membranes, batteries, supercapacitors, and electroactive polymers [30]. Recently,

nanocellulose has been shown to have great potential to produce flexible, transparent, smooth, and thermally stable substrates for printed electronics [31]. Polyethylene terephthalate (PET) film was used in this work as a plastic substrate because of its widespread use, e.g., for the manufacturing of flexible thin film cells for photovoltaic panels and as a first-choice material for a number of food and pharmaceutical packaging applications.

Here, we demonstrate that nanoindentation can be advantageously used for the nanomechanical characterization of thin coatings laid on a plastic film, enabling discrimination between the contribution of substrate and coating on the mechanical parameters for specific loading regimes. In addition, nanoindentation provides clear evidence of the reinforcing effect of NBBs on a local scale, while simultaneously allowing the identification of nanofiller types in a reliable fashion.

2. Theoretical background

In a typical nanoindentation experiment, a “loading-holding-unloading” cycle is carried out and a “loading vs. depth” plot obtained (Fig. 1a). Three-sided pyramid indenters (e.g., Berkovich indenters) find wide application due to geometrical reasons (e.g., self-similarity) and higher spatial resolution over other shapes [32]. The “compliance” method is frequently used to calculate hardness (H) and elastic modulus (E), relying on a number of theoretical models that assume a solely elastic behavior of the material during unloading (while deformation during loading is assumed to be both elastic and plastic). The Oliver and Pharr (OP) method is the most widely accepted nowadays [33]. Especially for elastic-plastic materials with limited pile-up (e.g., biopolymers), the OP method has been demonstrated to work better than other approaches for data treatment, becoming a primary technique for the mechanical investigation of thin films and small structural features [34]. For this reason, the OP method is integrated in the software-assisted procedure of most instrumental DSI equipment.

A cross-section of an indentation along with the parameters used in the OP theory is shown in Fig. 1b. According to the power law method [32], the upper portion of the unloading curve can be described by a power law relationship:

$$P = \alpha(h_{max} - h_f)^m \quad (1)$$

where P is the test load, h_{max} is the maximum indentation depth at the maximum loading (P_{max}), h_f is the permanent (or residual) indentation depth after the removal of the test force (plastic displacement), α is a constant, and m is a power law fitting constant related to material characteristics. For Berkovich indenters, m generally varies from 1.25 to 1.51. Note that the difference $h_{max} - h_f$ represents the elastic component of the displacement, i.e., the amount of displacement that is recovered by the material upon unloading (E_{rec} , Fig. 1b). h_f , α , and m are unknown quantities that can be determined by an initial second-degree fitting followed by an iterative procedure based on a least squares approach [3]. The slope of the initial (upper 10% to 50% of P_{max}) unloading curve intersecting the depth axis at h_c (see Fig. 1a) is defined as stiffness (S):

$$S = \left(\frac{dP}{dh}\right)_{max} = m \cdot P_{max} (h_{max} - h_f)^{-1} \quad (2)$$

The analysis of the first portion of the unloading part of the “load vs. displacement” curve can be used to calculate the reduced modulus (E_r), as defined by the following equation:

$$E_r = \frac{\sqrt{\pi} S}{2\beta \sqrt{A}} \quad (3)$$

where the β parameter is a correction factor that, for Berkovich indenters, has a value ranging between 1.0226 and 1.085, with 1.05 being the most suitable value for most materials [34]; A is the projected contact area determined from the indenter tip calibration. For a perfect Berkovich indenter, $A = 24.5 h_c^2$, with h_c (contact depth) defined as:

$$h_c = h_{max} - \frac{\varepsilon P_{max}}{S} \quad (4)$$

where h_{max} is the maximum displacement (see Fig. 1a, b) and ε is a geometrical constant related to the shape of the indenter [35]. In particular, $\varepsilon = 0.72$ for conical indenters, whereas it equals 0.75 and 1.00 for the paraboloid of revolution and flat punches, respectively. It is noted that the term $(\varepsilon P_{max})/S$ represents h_s in Fig. 1b, namely the displacement of the surface at the perimeter of the contact.

After gathering S and A from the indentation curve, the elastic modulus of the material (E) is derived using the following equation:

$$\frac{1}{E_r} = \frac{(1 - \nu^2)}{E} + \frac{(1 - \nu_i^2)}{E_i} \quad (5)$$

where ν and ν_i are the Poisson's ratio of the material and the indenter, respectively, whereas E_i is the elastic modulus of the indenter. Finally, the hardness (H) of the material can be calculated as:

$$H = \frac{P_{max}}{A} \quad (6)$$

Of interest is also the calculation of the components of the indentation work. The total mechanical work due to the indentation (W_{tot}) is composed of two terms, namely the plastic (irreversible) deformation work (W_{plast}) associated with the first loading part and the elastic (reversible) deformation (W_{elast}) owing to the removal of the test load (second part of the indentation curve), so that $W_{tot} = W_{plast} + W_{elast}$ (Fig. S1 of Supporting Information). By integrating the loading and unloading curves, it is easy to gather W_{tot} and W_{plast} and, by subtracting the latter from the former, W_{elast} can be eventually determined. The elastic contribution of the total indentation work (η) is then calculated as:

$$\eta = \frac{W_{elast}}{W_{tot}} \times 100 \quad (7)$$

In addition, the creep of a material (C) can be obtained keeping the test loading constant for a defined time span and calculating the change of the indentation depth as follows:

$$C = h_2 - h_1 \quad (8)$$

where h_1 is the indentation depth at the start of the pause and h_2 is the indentation depth at the end of the pause.

3. Experimental

3.1. Materials

Pullulan powder (PF-20 grade, Mn ~200 kDa) was purchased from Hayashibara Biochemical Laboratories Inc. (Okayama, Japan). Bindzil[®]15/500 (particle size: 5 nm; polydispersity index: 22.5%; dry matter: 15 wt%; specific surface area: 500 m² g⁻¹ at pH = 10.0), Bindzil[®]15/750 (particle size: 4 nm; polydispersity index: 22.4%; dry matter: 15 wt%; specific surface area: 750 m² g⁻¹ at pH = 10.5), and Bindzil[®] 2034 DI (particle size: 15 nm; polydispersity index: 27.3%; dry matter: 34 wt%; specific surface area: 200 m² g⁻¹ at pH = 2.8) colloidal silica nanoparticle water dispersions were purchased from AkzoNobel (Amsterdam, Netherlands) and coded as CS_{15/500}, CS_{15/750}, and CS₂₀₃₄, respectively. Cellulose nanocrystals (CNCs) were obtained by acid catalyzed hydrolysis according to the method used within our laboratory as described in a previous work [36]. The main physicochemical characteristics of the CNCs used in this work are fully described in previous papers [36–38]. One-side corona-treated PET A-410 (JBF RAK LLC, Ras Al Khaimah, United Arab Emirates) 12.0 ± 0.5 μm thick was kindly supplied by Metalvuoto spa (Roncello, Italy).

3.2. Methods and characterization

3.2.1. Coating preparation

A pristine pullulan solution (10.0 wt% wet basis), coded as P, was prepared by mixing the pullulan powder in cold water under gentle stirring (500 rpm) for 1 h at room temperature. Pullulan-colloidal silica dispersions were prepared by addition of an aliquot of the raw CS water dispersion in the pullulan solution so that a final CS concentration of 3 wt% (wet basis on the total weight, i.e., 30 wt% with respect to dry pullulan) was achieved for the three samples (i.e., P-CS_{15/500}, P-CS_{15/750}, and P-CS₂₀₃₄). In the same way, an aliquot of a freshly prepared CNC water dispersion was added to the pullulan solution to obtain a final CNC concentration of 0.3 wt% (wet basis on the total weight, i.e., 3.6 wt% with respect to dry pullulan) for the sample P-CNC. After mixing for 24 h at 500 rpm and 25 °C, all the formulations were left to rest for an additional 24 h before coating deposition. Milli-Q water (18.3 MΩ·cm) was used throughout the experiments.

3.2.2. Coating deposition

The deposition of the water dispersions on the corona-treated side of PET was performed using an automatic applicator (AB 3400, TQC B.V., Capelle aan den IJssel, The Netherlands) in accordance with the ASTM D823-07, Practice C, at a constant speed of 150 mm min⁻¹. In order to reset any possible difference arising from the different concentrations of the water dispersions, Mayer rods with selected engraved patterns were used. Two type B infra-red (IR) lamps of 1440 W (Helios Italquartz srl, Cambiagio, Italy) in combination with a constant and perpendicular flux of mild air (25.0 ± 0.3 °C for 2 min) at a distance of 40 cm from the applicator were used for solvent evaporation. A final dry thickness of 3.5 μm was achieved for all five dry coatings. All coated films were stored in a polycarbonate vacuum (-0.06 MPa) desiccator (Lab Companion line, Jeio Tech Co., Ltd., Daejeon, South Korea) under dry conditions for an additional two weeks before analyses.

3.2.3. Indentation test

The nanoindentation test was performed with a PB1000 Nanovea Mechanical Tester equipped with a Nano Module (Nanovea, Irvine, CA, USA). The use of the advanced Nano Module allowed

us to apply very low target loads, in the range of [40 μN – 400 mN], using a piezo driver while monitoring the load with an independent load cell and fine recording the position of the indenter inside the material with an independent capacitive depth sensor. A multichannel 24-bit acquisition card controlled every sensor and actuator. The samples were glued on sample holders and let dry for 30 minutes before testing in the environment enclosure of the instrument at 23 °C and 40% RH. For soft, thin film, it is important to apply very low loads and be able to monitor the position while applying, holding, and unapplying the load. To define the parameter of the test, we applied the widely adopted 10% rule [4]. Accordingly, in order to minimize the effect of the substrate properties of the measurement of the film properties, the indentation depth should be no more than 10% of the film thickness. This rule has its basis in the determination of hardness testing, where the intention is to restrict the extent of the plastic zone to the film material. To demonstrate the absence of any interference of the PET substrate on the coating's properties, we first gathered the hardness value (H , MPa) of the PET-coated surfaces (i.e., both the coating surface and the PET surface) and of the bare (i.e., uncoated) PET surface through nanoindentation tests with the following testing conditions: maximum load 0.2 mN; indentation depth 120 nm; and loading/unloading rate 800 $\mu\text{N}/\text{min}$. Second, we performed the same test as above but at different maximum loadings (0.1 mN, 0.2 mN, 0.3 mN, 0.5 mN, 0.7 mN, 1.0 mN, and 1.2 mN), with the goal of pinpointing the depth boundary for an independent measurement of the coating's nanomechanical properties.

To evaluate both the mechanical properties and distribution effects (e.g., the uniformity of the fillers in the polymeric matrix or the presence of surfacing nanoparticles), and taking into account the morphological differences between the fillers, two different test conditions were set, as reported in Table 1. A reference sample of a pure pullulan film was used in both steps. In step 1, the tests were performed in a matrix of 10 \times 8 indentations with a spacing of 0.3 μm in depth control at the maximum depth of 40 nm. In this way, we made sure that the indentations were reciprocally independent, i.e., the area on each individual indentation cycle was not influenced by the previous cycle. In step 2, because of the larger average size of the fillers, we decided to perform the tests in a

matrix of 6×6 indentations with a spacing of 1 μm in load control at a maximum load of 200 μN . Poisson's ratio of the material (ν) and the indenter (ν_i) were fixed at 0.3 and 0.2, respectively.

3.2.4. 2D and 3D plots of mechanical data

2D and 3D maps of elastic modulus (E , GPa), hardness (H , MPa), and creep (C , nm) were obtained using the command-line driven graphing utility Gnuplot 5.0. In the maps, different colors denote different values of the investigated parameter (E , H , or C) as collected from the matrix of the indentation tests. Therefore, each plot carries only the information related to the mechanical properties of the material in each testing site for the chosen matrix, i.e., the mechanical properties of the testing area for each material.

3.2.5. ζ -potential of nanoparticles

Nanocolloidal dispersions were characterized in terms of electrokinetic potential through phase analysis light scattering (PALS) technology using a particle analyzer Litesizer 500 (Anton Paar, Graz, Austria). ζ -potential (mV) and conductivity (mS/cm) of "as-received" nanocolloidal water dispersions were determined at 25.0 ± 0.1 °C by means of a 35 mW diode laser ($\lambda = 658$ nm) and at a 15° detection angle.

3.2.6. Statistical analysis

The statistical significance of the differences in films' properties and behavior was determined via one-way analysis of variance using StatgraphicsPlus 4.0 software (STSC, Rockville, MD, USA). The mean values, where appropriate, were separated by a least significant difference (LSD) multiple range test at $p < 0.05$.

4. Results and Discussion

4.1. Influence of the plastic substrate

A first set of experiments was carried out on the coated PET samples and bare PET. The hardness values of the coatings, of the PET surface supporting the coating, and of the bare PET are reported in Table 2. For the three coating surfaces, H was significantly lower compared to the same parameter calculated for the plastic substrate. Interestingly, the bare PET surface exhibited a higher H value compared to the same surface coated with the three different coating formulations (i.e., P, P-CNC, and P-CS₂₀₃₄). A tentative explanation for this observation could be related to the absorption of water molecules by the PET upon coating deposition, with subsequent deterioration of the mechanical performance of the plastic material.

In order to clarify the effect of the indentation loading, the indentation test described above was repeated using the same setting, but at seven different loads. The values of H and the penetration depth as a function of the maximum loads for the coating P-CNC are displayed in Fig. 2. The S-shaped plot indicates that for low loadings (i.e., 0.1 mN and 0.2 mN) the value of hardness (~ 31 MPa) solely relates to the coating. In other words, even a 100% increase in the load applied on the coating surface did not affect the final H value significantly (while a significant increase in the penetration depth from 116.7 nm to 155.5 nm was observed). As the loading values were increased, a convolution of the effect “substrate + coating” was disclosed by approaching the H value of the substrate (~ 470 MPa). Indeed, for loads > 0.3 mN, the recorded values of H exceeded 500 MPa, suggesting the reinforcing effect of the coating on the hardness performance of the material. Eventually, a plateau was reached when the H values did not change any longer for any further increase in the load applied (at least within the maximum loading range investigated).

It can therefore be concluded that the indentation test is able to discriminate between plastic substrate and coating, provided that an adequate setup is appropriately fixed. More specifically, for indentation loads < 0.2 mN and penetration depths < 155 nm, the nanomechanical behavior of the coating is independent from the substrate. Above those values, the influence of the substrate starts to affect the overall measurement, leading to an overestimation of the hardness of the coating.

4.2. First step – size effect

In the first step of the experiment, we compared the pristine pullulan coating and the bionanocomposite coatings P-CS_{15/500} and P-CS_{15/750} in order to test the capability of the nanoindentation approach to i) detect differences arising from the addition of the silica nanoparticles in the main biopolymer phase and ii) discriminate between nanoparticles of the same shape but different size and surface area (4 and 5 nm, with 500 and 750 m²/g, respectively). The “load-penetration depth” curves of samples P, P-CS_{15/500}, and P-CS_{15/750} are displayed in Fig. S2 of Supporting Information. From these curves, which are typical of elastic-plastic modes of deformation, both E (GPa) and H (MPa) parameters were calculated for the three coating samples, as reported in Table 3. There was a significant difference between the three samples as far as both E and H are concerned. In particular, sample P exhibited the lowest hardness and elastic modulus values, while sample P-CS_{15/500} showed the highest elastic modulus and sample P-CS_{15/750} showed the highest hardness. This was reflected in the final total work induced by the indentation on the samples’ surfaces (Fig. 3a), with W_{tot} equal to 0.228 ± 0.014 pJ, 0.284 ± 0.016 pJ, and 0.314 ± 0.020 pJ for samples P, P-CS_{15/500}, and P-CS_{15/750}, respectively. It is interesting to note that the elastic part of the indentation work (η) scaled proportionally with W_{tot} values (Fig. 3b), accounting for ~ 27%, ~ 31%, and ~ 34% of the total work for samples P, P-CS_{15/500}, and P-CS_{15/750}, respectively.

For a better interpretation of these results, we have generated the 3D plots of H distribution on a representative surface of $2.70 \times 2.10 \mu\text{m}^2$ for the three samples (Fig. 4). There is an obvious difference between the bare pullulan coating on one hand and the two nanocomposite coatings on the other hand, the former having a more even (besides lower) hardness distribution compared to the composite formulations. Irrespective of the type of particles loaded in the main biopolymer phase, the addition of colloidal silica had a significant reinforcing effect on the matrix, as demonstrated by the overall increase of H values (compare the green background of samples P-CS_{15/500} and P-CS_{15/750} with the blue background of sample P). Furthermore, the surface of sample P-CS_{15/500} (Fig. 4, center) revealed a more homogeneous distribution of the nanoparticles compared

with sample P-CS_{15/750} (Fig. 4, right), which exhibited a more spiked pattern. Apparently, the addition of smaller particles with higher surface area drove the formation of larger domains separated from the main biopolymer matrix. The extensive clustering observed for sample P-CS_{15/750} is therefore suggested to explain its higher hardness values. These results confirm previous findings on the effect of CS nanoparticles loaded in fossil-based polymer matrices [5]. Overall, the reinforcing effect of CS nanoparticles observed in this work is within the same order of magnitude as the values recorded for both thermoset (e.g., epoxy and polyacrylates) and thermoplastic matrices. As far as the latter are concerned, Bhattacharya and Chaudhry fabricated biocompatible nanocomposites made of silica-reinforced poly (vinyl alcohol (PVA) [39], to which pullulan has been approached for many different physicochemical properties [40]. The highest indentation modulus of 8.1 GPa was in line with the P-CS samples tested in this study. However, this value was obtained for the nanocomposite with 54.6 wt% nanosilica, whereas E for the nanocomposite with 28.1 wt% silica (i.e., a concentration similar to that used in this study) decreased to 3.4 GPa. This difference can be first explained considering the very low E value (0.3 GPa) found for the neat polymer (PVA) compared with the pristine pullulan coating tested here (~ 6.3 GPa). In addition, the authors used 80 nm average diameter silica nanoparticles and poly(allylamine hydrochloride) (PAH) as a counter ion of the negatively charged silica nanoparticles to prevent their aggregation.

4.3. Second step – shape effect

In the second part of our investigation, we carried out a series of experiments to compare the impact of rod-like and spherical nanoparticles (cellulose nanocrystals and colloidal silica, respectively) on the main pullulan phase. The E and H values extrapolated from the “load-displacement” indentation curves for the three different coatings are reported in Table 3. There was a significant difference between the three samples with regard to the H parameter. While the bare pullulan coating (sample P) was the softer one, the addition of spherical nanoparticles (sample P-CS₂₀₃₄) apparently had a greater effect on the surface hardness compared to the cellulose

nanowhiskers (sample P-CNC). However, the same conclusion cannot be drawn for the E parameter because the addition of colloidal silica did not result in any apparent improvement compared with both the bare pullulan coating and the coating loaded with CNCs. Conversely, the P-CNC coating exhibited E values significantly higher than P, reflecting the high elastic modulus of CNCs (the average value being around 130 GPa) [41], which is one of the most attractive mechanical features of these nanoparticles [42]. We have explained these results in terms of the different distribution of the NBBs within the main biopolymer matrix. Regarding to this scope, we have generated 2D maps of the three parameters quantified within this second step of the investigation—namely, elastic modulus, hardness, and creep—on representative $6 \times 6 \mu\text{m}^2$ surfaces for the three samples (Fig. 5). If we look at the maps of H , which better reflects the local distribution of the individual phases (i.e., biopolymer and NBBs), we can notice the well-defined “two-color” pattern for sample P-CS₂₀₃₄ (row b, right column of Fig. 5) compared to the evenly colored pattern of sample P (row b, left column of Fig. 5) and the randomly colored pattern of sample P-CNC (row b, center column of Fig. 5).

Such a “two-color” pattern stems from a nonuniform distribution of CS nanoparticles, which in turn gives rise to local aggregation and clustered silica domains (the “down” orange part of the panel) as compared with unloaded (i.e., pristine) pullulan regions (the “up” violet part of the panel). This behavior, which was not observed for the colloidal silica nanoparticles used in the first step of this work, was detected throughout the indentation experiments on the P-CS₂₀₃₄ surface. This apparent discrepancy between CS types, besides the size effect of the starting spherical particles, can be plausibly explained in terms of surface chemistry. While CS_{15/500} and CS_{15/750} are anionic nanoparticles (i.e., the net negative charge can play a role in preventing cluster formation, or aggregation), CS₂₀₃₄ are zero-charge nanoparticles (i.e., particle aggregation by, e.g., hydrogen bonding is favored). More specifically, the measured ζ -potential of the CS_{15/500} and CS_{15/750} colloidal dispersions was -45.9 ± 1.1 mV and -15.2 ± 0.7 mV, whereas the ζ -potential of the

CS₂₀₃₄ sample was -1.8 ± 0.3 mV (see Fig. S3). The different electric behavior of the three colloidal silica nanoparticles is also confirmed by the conductivity values, which were equal to 4.417 mS/cm, 7.010 mS/cm, and 0.599 mS/cm according to the light scattering experiments. This would explain a co-continuous structure with that of pullulan for CS_{15/500} and CS_{15/750} nanoparticles on one hand a more clustered morphology due to small aggregates for CS₂₀₃₄ nanoparticles. The impact of the nanoparticle distribution on the local mechanical properties of the nanocomposite coatings is further evidenced if one considers the contribution of the two distribution regions on the overall value of both E and H . As clearly shown in Fig. 6, the “up” part of the panel (namely the CS-poor region) exhibits nanomechanical features very similar to those of the bare pullulan coating (6.95 ± 0.77 GPa and 296.25 ± 59.83 MPa for E and H , respectively) insomuch as the two data sets can be superimposed. On the contrary, the “down” part of the panel (namely the CS-rich region) gives rise to a data cloud shifted to higher values for both E and H (7.70 ± 0.65 GPa and 410 ± 58.55 MPa, respectively).

A different scenario was disclosed as far as the C parameter is concerned. The average creep value (i.e., the indentation depth calculated after applying a load of ~ 195 μ N) is significantly lower for the coating P-CS₂₀₃₄ (16.5 ± 1.85 nm) compared with the coating surfaces P (21.07 ± 2.46 nm) and P-CNC (21.33 ± 3.90), irrespective of the specific zone of the indented areas (Fig. 7). This is confirmed by the creep map of the sample P-CS₂₀₃₄ in Fig. 5 (line c, right column), where a homogeneously colored violet surface can be detected. These results can be explained considering the maximum load of 200 μ N set for the second step of the analysis. This means that C can be affected by the z -axis distribution of the NBBs. Because of morphology effects (geometry and dimensions), it is plausible that CS nanoparticles fell into the pullulan matrix to a higher extent than CNCs, which would explain the lower sensitivity of the P-CS₂₀₃₄ coating to compressive stresses. These observations support the idea that the C value relies more on a mean distribution of the nanoparticles at a microscale, rather than on local gradients, which instead was observed for both E and H . Therefore, the addition of CS nanoparticles, although not homogeneously dispersed in the

main biopolymer matrix, yielded a more cohesive surface, while CNCs did not result in any significant difference in terms of creep as compared with the pristine pullulan coating surface.

This can be ascribed to the lower effective surface area of CNCs than of CS nanoparticles, as pointed out by Brinkmann *et al.* [43]. The surface area of CNCs dispersed in water can be a few hundred m^2/g , the variability depending on the size distribution of the crystals; for example, the expected surface area range for particles with average lengths and cross sections of 100-200 nm and 4-5 nm, respectively, can be estimated to be between 400 and 500 m^2/g . In reality, the surface area dramatically decreases (up to even two orders of magnitude lower) for dry aggregated CNCs, as demonstrated by Olsson *et al.* for dry bacterial nanocellulose (surface area $\sim 100 \text{ m}^2/\text{g}$) [44]. The solvent removal during the preparation of thin films and coatings (as in this work) promotes the formation of aggregates or agglomerates with a very small accessible surface area, which in turn would affect the interaction at the interface with the main polymer matrix (e.g., pullulan molecular chains in this work).

5. Conclusions

As confirmed by recent works [see ref. 6], nanoindentation is a versatile instrumental approach for in-depth mechanical characterization of a material's surface at the local level, i.e., at the nanometer scale. The rising interest in biopolymer systems has prompted scientists to expand the use of this technique beyond conventional applications on fossil-based materials. Nanoindentation, in particular, is increasingly used in the field of bionanocomposite materials, for which understanding the interface/interphase nature is crucial in order to fully exploit the size effect of the nanoparticles with the ultimate goal of improving the final performance of the biopolymer phase. However, according to the literature, the information on the use of nanoindentation for bionanocomposite materials pertains almost exclusively to stand-alone films [45–50]. In practice, today's market applications (e.g., displays, photovoltaic cells, and packaging materials) employ biopolymer nanocomposites in the form of thin films and coatings laid on a supporting substrates,

in most cases flexible materials such as plastics [14]. Duan *et al.* dealt with nanoindentation experiments on thin biopolymer composites, but they focused primarily on the development of analytical models to study how the elastic modulus changes with the penetration for simple composite materials [51].

In this work, we used nanoindentation to gather nanomechanical information of biopolymer nanocomposite coatings deposited on a plastic film. First, we provided evidence that the substrate's mechanical properties do not affect the mechanical characterization of the coating if a suitable instrumental setup is pinpointed. Second, the addition of NBBs to generate bionanocomposite coatings was successfully discriminated from the bare biopolymer system, and new nanomechanical features, quantified in terms of elastic modulus, hardness, and creep, were described. The impact of NBBs geometry on the nanomechanical performance of the final nanocomposite coatings was also addressed in light of some surface chemistry considerations. This has revealed unexpected behaviors for round-shaped NBBs, for which the local distribution played a crucial role in the hardness performance, whereas it turned out to be less influential on the overall creep behavior of the material. In the same way, it was clarified that the reinforcement of the pullulan coatings loaded with CNCs can be plausibly attributed to the high elastic modulus of the individual crystals dispersed in the main polymer matrix. However, the low accessibility of the surface area of dry CNCs (and thus the reduced interaction with the main pullulan phase) may explain the inferior creep performance of the same bionanocomposite surface.

The findings arising from this work may represent a step forward to expand the use of nanoindentation for the special application on bionanocomposite coatings deposited on relatively thin and flexible substrates, e.g., plastics, while gaining a better fundamental physical understanding of the local mechanical behavior of the coating interphases and their relationship with the substrate underneath.

Acknowledgments

The authors acknowledge the support of the University of Milan “Research Support Plan 2015–2017”, Line 2, grant # 15-6-3024000-402.

References

- [1] C. A. Schuh, Nanoindentation Studies of Materials, *Mater. Today* 9 (2006) 32–40.
- [2] D. M. Ebenstein, K. J. Wahl, A comparison of JKR-based methods to analyze quasi-static and dynamic indentation force curves, *J. Colloid Interface Sci.* 298 (2006) 652–662.
- [3] Y. T. Cheng, C. M. Cheng, Scaling, Dimensional Analysis, and Indentation Measurements, *Mater. Sci. Eng. R* 44 (2004) 91–149.
- [4] A. C. Fischer-Cripps, Critical Reviews of Analysis And Interpretation of Nanoindentation Test Data, *Surf. Coat. Technol.* 200 (2006) 4153–4165.
- [5] N. A. Sakharova, J. V. Fernandes, J. M. Antunes, M. C. Oliveira, Comparison Between Berkovich, Vickers and Conical Indentation Tests: A Three-Dimensional Numerical Simulation Study, *Int. J. Solids Struct.* 46 (2009) 1095–1104.
- [6] A. M. Díez-Pascual, M. A. Gómez-Fatou, F. Ania, A. Flores, Nanoindentation in Polymer Nanocomposites, *Prog. Mater. Sci.* 67 (2015) 1–94.
- [7] J. Shao, Y. Wang, X. Chen, X. Hu, C. Du, Nanomechanical Properties of Poly(L-Lactide) Nanofibers After Deformation, *Colloids Surf., B.* 120 (2014) 97–101.
- [8] B. Das, K. E. Prasad, U. Ramamurty, C. N. R. Rao, Nano-Indentation Studies on Polymer Matrix Composites Reinforced by Few-Layer Graphene, *Nanotechnology* 20 (2009) 125705–125710.

- [9] A. Flores, M. Naffakh, A. M. Díez-Pascual, F. Ania, M. A. Gómez-Fatouk, Evaluating the Reinforcement of Inorganic Fullerene-Like Nanoparticles in Thermoplastic Matrices by Depth-Sensing Indentation, *J. Phys. Chem. C* 117 (2013) 20936–20943.
- [10] N. Funk, M. Vera, L. J. Szewciw, F. Barthelat, M. P. Stoykovich, F. J. Vernerey, Bioinspired Fabrication and Characterization of a Synthetic Fish Skin for the Protection of Soft Materials, *ACS Appl. Mater. Interfaces* 7 (2015) 5972–5983.
- [11] E. Callard Preedy, S. Perni, P. Prokopovich, Cobalt and Titanium Nanoparticles Influence on Mesenchymal Stem Cell Elasticity and Turgidity, *Colloids Surf., B*. 157 (2017) 146–156.
- [12] N. Wang, A.-M. Trunfio-Sfarghiu, D. Portinha, S. Descartes, E. Fleury, Y. Berthier, J.-P. Rieu, Nanomechanical and Tribological Characterization of the MPC Phospholipid Polymer Photografted onto Rough Polyethylene Implants, *Colloids Surf., B*. 108 (2013) 285–294.
- [13] C. Stauch, T. Ballweg, W. Stracke, R. Luxenhofer, K. Mandel, Burstable Nanostructured Micro-Raspberries: Towards Redispersible Nanoparticles from Dry Powders, *J. Colloid Interface Sci.* 490 (2017) 401–409.
- [14] I. U. Unalan, G. Cerri, E. Marcuzzo, C. A. Cozzolino, S. Farris, Nanocomposite Films and Coatings Using Inorganic Nanobuilding Blocks (NBB): Current Applications and Future Opportunities in the Food Packaging Sector, *RSC Adv.* 4 (2014) 29393–29428.
- [15] J. W. Rhim, H. M. Park, C. S. Ha, Bio-Nanocomposites for Food Packaging Applications, *Prog. Polym. Sci.* 38 (2013) 1629–1652.
- [16] G. Kickelbick, Concepts for the Incorporation of Inorganic Building Blocks into Organic Polymers on a Nanoscale, *Prog. Polym. Sci.* 28 (2003) 83–114.
- [17] J. M. Fuentes-Alventosa, L. Introzzi, N. Santo, G. Cerri, A. Brundu, S. Farris, Self-Assembled Nanostructured Biohybrid Coatings by an Integrated ‘Sol-Gel–Intercalation’ Approach, *RSC Adv.* 3 (2013) 25086–25096.

- [18] S. Farris, L. Introzzi, J. M. Fuentes-Alventosa, N. Santo, R. Rocca, L. Piergiovanni, Self-Assembled Pullulan-Silica Oxygen Barrier Hybrid Coatings for Food Packaging Applications, *J. Agric. Food Chem.* 60 (2012) 782–790.
- [19] L. Introzzi, T. O. J. Blomfeldt, S. Trabattoni, S. Tavazzi, N. Santo, A. Schiraldi, L. Piergiovanni, S. Farris, Ultrasound-Assisted Pullulan/Montmorillonite Bionanocomposite Coating with High Oxygen Barrier Properties, *Langmuir* 28 (2012) 11206–11214.
- [20] B. X. Du, J. Li, W. Du, Surface Charge Accumulation and Decay on Direct fluorinated Polyimide/Al₂O₃ Nanocomposites, *IEEE T. Dielect. El. In.* 20 (2013) 1764–1771.
- [21] A. Allahverdi, M. Ehsani, H. Janpour, S. Ahmadi, The Effect of Nanosilica on Mechanical, Thermal and Morphological Properties of Epoxy Coating, *Prog. Org. Coat.* 75 (2012) 543–548.
- [22] P. Dais, S. Vlachou, F. Tavel, ¹³C Nuclear Magnetic Relaxation Study of Segmental Dynamics of the Heteropolysaccharide Pullulan in Dilute Solutions, *Biomacromolecules* 2 (2001) 1137–1147.
- [23] L. Introzzi, J. M. Fuentes-Alventosa, C. A. Cozzolino, S. Trabattoni, S. Tavazzi, C. L. Bianchi, A. Schiraldi, L. Piergiovanni, S. Farris, ‘Wetting enhancer’ Pullulan Coating for Antifog Packaging Applications, *ACS Appl. Mater. Interfaces* 4 (2012) 3692–3700.
- [24] R. E. Patterson, Preparation and Uses of Silica Gels and Precipitated Silicas. In *Colloidal silica: Fundamentals and Applications*; H. E. Bergna, W. O. Roberts, (Eds.), CRC Press: Boca Raton, FL. 131 (2005) 779–788.
- [25] A. Dufresne, *Nanocellulose: From Nature to High Performance Tailored Materials*; Walter de Gruyter GmbH: Berlin (2013).
- [26] F. Ullmann, M. Bohnet, *Ullmann’s encyclopedia of industrial chemistry*, 7th ed.; J. Wiley & Sons: Weinheim, NY (2009).

- [27] H. Zou, S. Wu, J. Shen, Polymer/Silica Nanocomposites: Preparation, Characterization, Properties, and Applications, *Chem. Rev.* 108 (2008) 3893–3957.
- [28] Q. Lin, S. A. Cohen, L. Gignac, B. Herbst, D. Klaus, E. Simonyi, J. Hedrick, J. Warlaumont, H-J. Lee, W-L. Wu, Low Dielectric Constant Nanocomposite Thin Films Based on Silica Nanoparticle and Organic Thermosets, *J. Polym. Sci. Part B Polym. Phys* 45 (2007) 1482–1493.
- [29] T. Abitbol, A. Rivkin, Y. Cao, Y. Nevo, E. Abraham, T. Ben-Shalom, S. Lapidot, O. Shoseyov, Nanocellulose, a Tiny Fiber with Huge Applications, *Curr. Opin. Biotech.* 39 (2016) 76–88.
- [30] R. J. Moon, A. Martini, J. Nairn, J. Simonsen, J. Youngblood, Cellulose Nanomaterials Review: Structure, Properties and Nanocomposites, *Chem. Soc. Rev.* 40 (2011) 3941–3994.
- [31] F. Hoeng, A. Denneulin, J. Bras, Use of Nanocellulose in Printed Electronics: a review, *Nanoscale* 8 (2016) 13131–13154.
- [32] M. F. Doerner, W. D. Nix, A Method for Interpreting the Data from Depth-Sensing Indentation Instruments, *J. Mater. Res.* 1 (1986) 601–609.
- [33] W. C. Oliver, G. M. Pharr, An Improved Technique for Determining Hardness and Elastic Modulus Using Load Displacement Sensing Indentation Experiments, *J. Mater. Res.* 7 (1992) 1564–1583.
- [34] W. C. Oliver, G. M. Pharr, Measurement of Hardness and Elastic Modulus by Instrumented Indentation: Advances in Understanding and Refinements to Methodology, *J. Mater. Res.* 19 (2004) 3–20.
- [35] M. Martin, M. Troyon, Fundamental Relations Used in Nanoindentation: Critical Examination Based on Experimental Measurements, *J. Mater. Res.* 17 (2002) 2227–2234.

- [36] F. Li, P. Biagioni, M. Finazzi, S. Tavazzi, L. Piergiovanni, Tunable Green Oxygen Barrier Through Layer-By-Layer Self-Assembly of Chitosan and Cellulose Nanocrystals, *Carbohydr. Polym.* 92 (2013) 2128–2134.
- [37] F. Li, P. Biagioni, M. Bollani, A. Maccagnan, L. Piergiovanni, Multi-Functional coating of Cellulose Nanocrystals for Flexible Packaging Applications, *Cellulose* 20 (2013) 2491–2504.
- [38] F. Li, E. Mascheroni, L. Piergiovanni, The Potential of Nanocellulose in the Packaging Field: A Review, *Packag. Technol. Sci.* 28 (2015) 475–508.
- [39] M. Bhattacharya, S. Chaudhry, High-Performance Silica Nanoparticle Reinforced Poly (Vinyl Alcohol) as Templates for Bioactive Nanocomposites, *Mater. Sci. Eng. C* 33 (2013) 2601–2610.
- [40] S. Farris, I. U. Unalan, L. Introzzi, J. M. Fuentes-Alventosa, C. A. Cozzolino, Pullulan-Based Films and Coatings for Food Packaging: Present Applications, Emerging Opportunities, and Future Challenges, *J. Appl. Polym. Sci.* 131 (2014) 40539–40551.
- [41] A. Dufresne, Nanocellulose: A New Ageless Bionanomaterial, *Mater. Today* 16 (2013) 220–227.
- [42] Y. Habibi, L. A. Lucia, O. J. Rojas, Cellulose Nanocrystals: Chemistry, Self-Assembly, and Applications, *Chem. Rev.* 110 (2010) 3479–3500.
- [43] A. Brinkmann, M. Chen, M. Couillard, Z. J. Jakubek, T. Leng, L. J. Johnston, Correlating Cellulose Nanocrystal Particle Size and Surface Area, *Langmuir* 32 (2016) 6105–6114.
- [44] R. T. Olsson, M. A. S. Azizi Samir, G. Salazar Alvarez, L. Belova, V. Strom, L. A. Berglund, O. Ikkala, J. Nogues, U. W. Gedde, Making Flexible Magnetic Aerogels and Stiff Magnetic Nanopaper Using Cellulose Nanofibrils as Templates, *Nat. Nanotechnol.* 5 (2010) 584–588.

- [45] J. Sahari, S. M. Sapuan, E. S. Zainudin, M. R. Ishak, M. A. Maleque, M. Y.M. Zuhri, R. Akhtar, Nanoindentation and the Low Velocity Impact Response of Biofibre, Biopolymer and its Biocomposite Derived from Sugar Palm Tree, *Curr. Org. Synth.* 14 (2017) 227–232.
- [46] A. Rath, S. Mathesan, P. Ghosh, Nanomechanical Characterization and Molecular Mechanism Study of Nanoparticle Reinforced and Cross-Linked Chitosan Biopolymer, *J. Mech. Behav. Biomed. Mater.* 55 (2016) 42–52.
- [47] S. Rjafiallah, N. Benseddiq, S. Guessasma, Effect of Interface Properties on the Effective Properties of Biopolymer Composite Materials, *Mat.-wiss. u. Werkstofftech.* 41 (2010) 265–269.
- [48] S. Guessasma, M. Sehaki, D. Lourdin, A. Bourmaud, Viscoelasticity Properties of Biopolymer Composite Materials Determined Using Finite Element Calculation and Nanoindentation, *Comput. Mater. Sci.* 44 (2008) 371–377.
- [49] D. Verma, K. S. Katti, D. R. Katti, B. Mohanty, Mechanical Response and Multilevel Structure of Biomimetic Hydroxyapatite/Polygalacturonic/Chitosan Nanocomposites, *Mater. Sci. Eng. C* 28 (2008) 399–405.
- [50] S.-F. Wang, L. Shen, W.-D. Zhang, Y.-J. Tong, Preparation and Mechanical Properties of Chitosan/Carbon Nanotubes Composites, *Biomacromolecules* 6 (2005) 3067–3072.
- [51] P. Duan, S. Bull, J. Chen, Modeling the Nanomechanical Responses of Biopolymer Composites During the Nanoindentation, *Thin Solid Films* 596 (2015) 277–281.

Figure captions

Fig. 1. (a) Idealized load-displacement indentation curve. (b) Exemplification of the cross-sectional profile during a loading-unloading indentation cycle with some relevant parameters (adapted from ref. 33).

Fig. 2. Hardness (H , MPa) and penetration depth (nm) as a function of the maximum load (mN) on the surface of the coating P-CNC deposited on the PET plastic substrate.

Fig. 3. (a) Total work (W_{tot}) and (b) elastic part of the indentation work (η) obtained from 80 indentation cycles on samples P (—), P-CS_{15/500} (—), and P-CS_{15/750} (—).

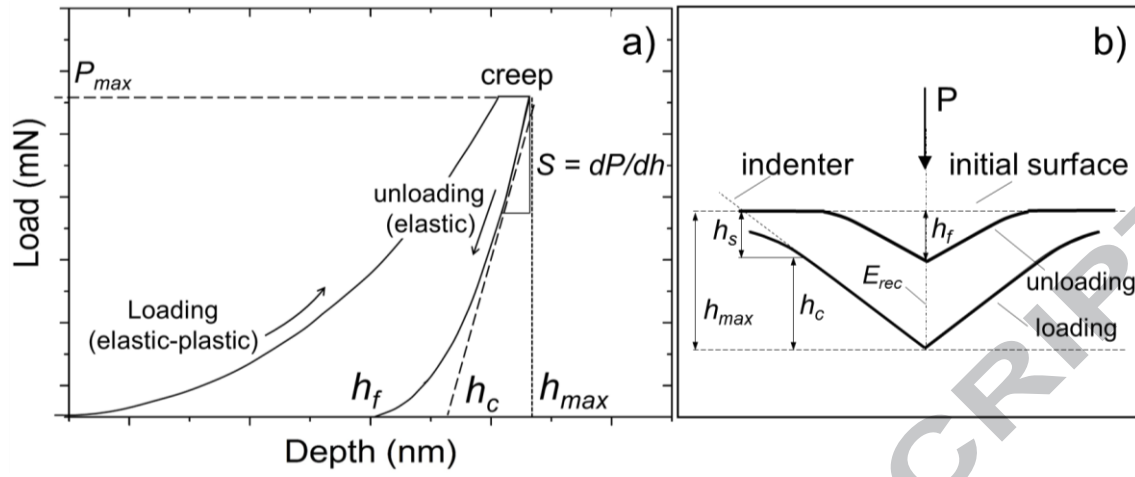
Fig. 4. Three-dimensional images of hardness (H , MPa) distribution on representative portions ($2.70 \times 2.10 \mu\text{m}^2$) of the coating surface of samples P (left), P-CS_{15/500} (center), and P-CS_{15/750} (right).

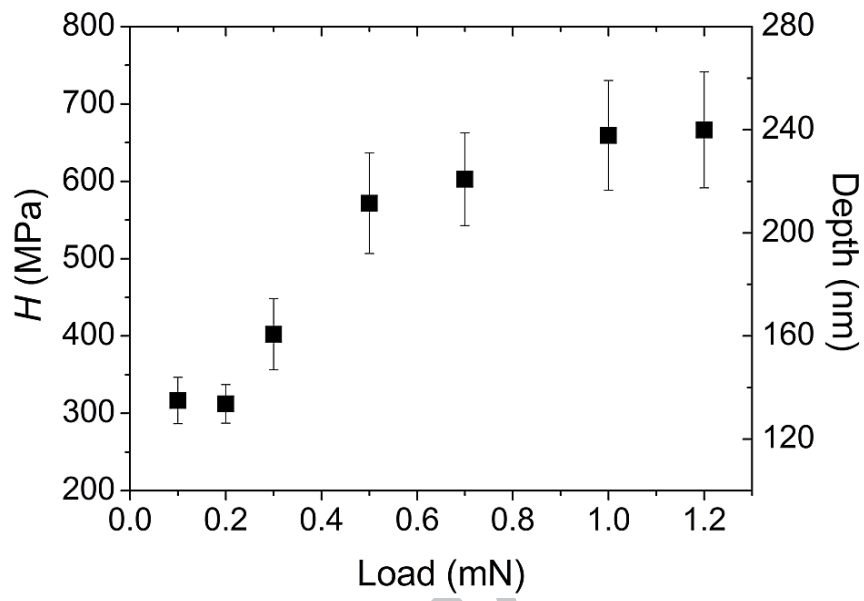
Fig. 5. Two-dimensional maps of (a) elastic modulus (E , GPa), (b) hardness (H , GPa), and (c) creep (C , nm) distribution on representative portions ($6 \times 6 \mu\text{m}^2$) of the coating surface of samples P (left), P-CNC (center), and P-CS₂₀₃₄ (right).

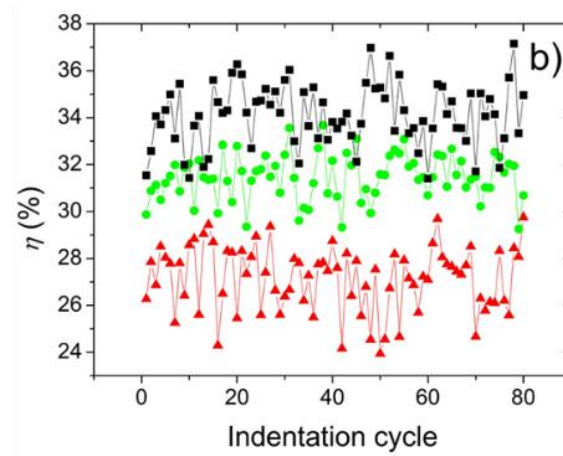
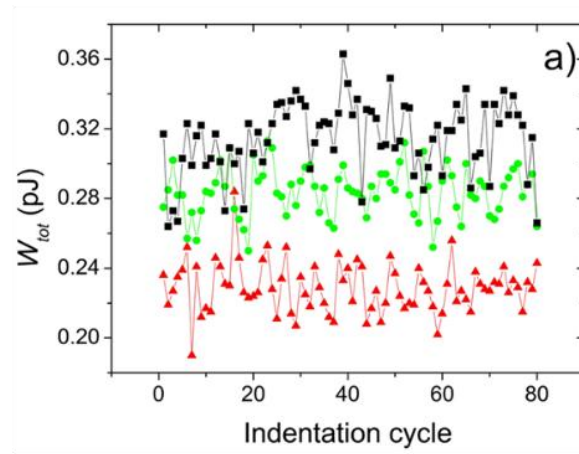
Fig. 6. “Hardness vs. elastic modulus” plots for the coatings P (—), P-CS₂₀₃₄ – “up” region (—), and P-CS₂₀₃₄ – “down” region (—).

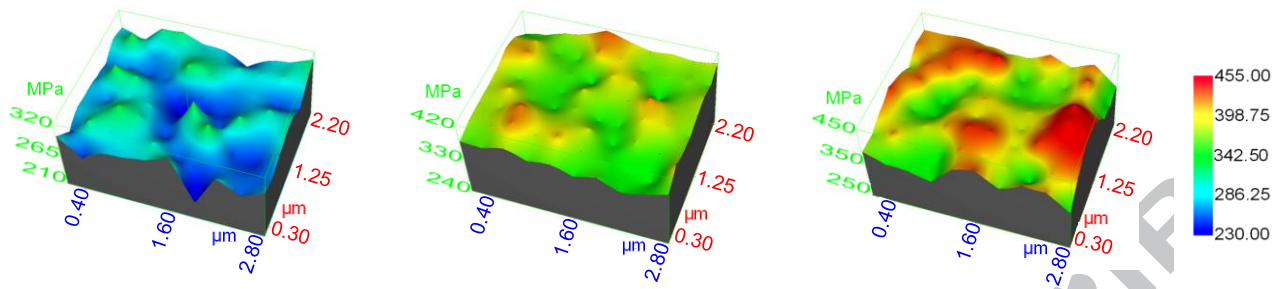
Fig. 7. “Creep vs. maximum force” for the coatings P (—), P-CNC (—), and P-CS₂₀₃₄ – “up” region (—). Error bars are for standard deviations.

ACCEPTED MANUSCRIPT

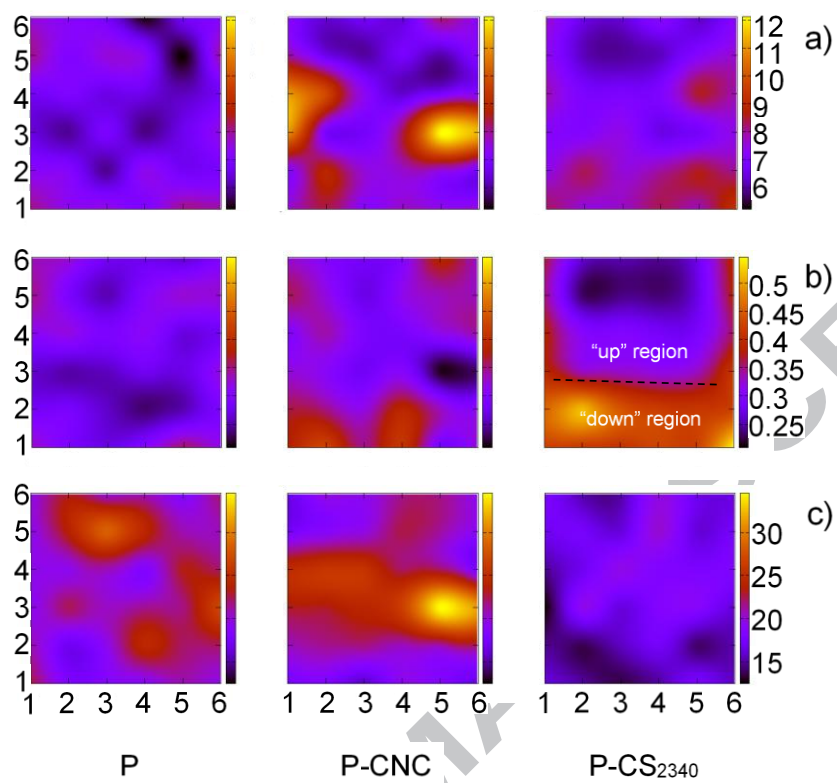


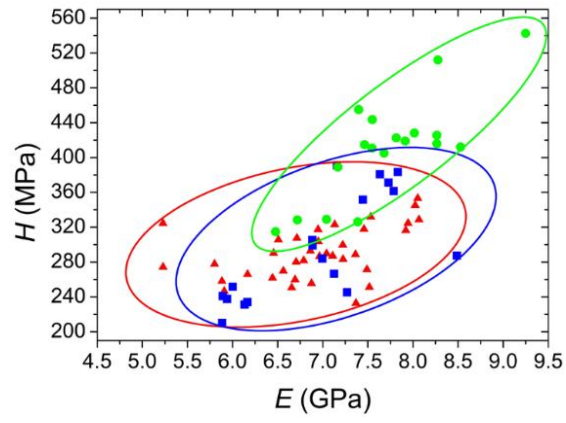




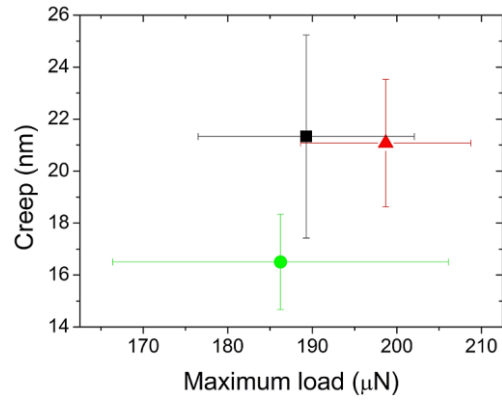


ACCEPTED MANUSCRIPT





ACCEPTED MANUSCRIPT



ACCEPTED MANUSCRIPT

Table 1. Main parameters set for step 1 and step 2 of the indentation test.

Parameter	Value
Step 1	
Loading	Linear
Control	Depth Control
Indenter	Berkovich
Max Depth	40 [nm]
Pause at Max Load	10 [s]
Loading Rate	800 [$\mu\text{N}/\text{min}$]
Unloading Rate	800 [$\mu\text{N}/\text{min}$]
Step 2	
Loading	Linear
Control	Load Control
Indenter	Berkovich
Max Load	200 [μN]
Pause at Max Load	10 [s]
Loading Rate	800 [$\mu\text{N}/\text{min}$]
Unloading Rate	800 [$\mu\text{N}/\text{min}$]

Table 2. Hardness (H , MPa) values obtained after “loading-holding-unloading” indentation test on the coated PET samples (both PET and coating surfaces) and bare (uncoated) PET.

Type of test	Sample		
	P	P-CNC	P-CS ₂₀₃₄
coated PET (coating surface)	285.74 ± 25.87^a	316.32 ± 32.13^c	360.65 ± 44.05^d
coated PET (PET surface)	462 ± 2.95^b	463.62 ± 2.29^b	465 ± 2.05^b
uncoated PET		472.59 ± 1.60^c	

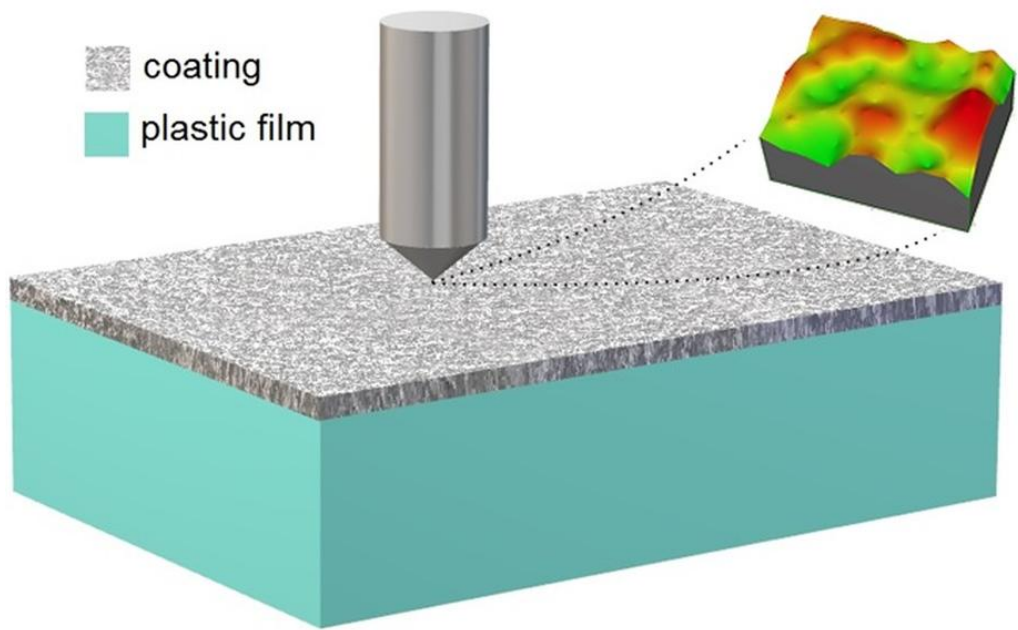
Results are expressed as mean values and standard deviation. Different superscripts within a group (i.e., within each parameter for each step) refer to a statistically significant difference ($p < 0.05$).

Table 3. Elastic modulus (E) and hardness (H) obtained from the nanoindentation tests on the different coating surfaces.

Coating sample	E (GPa)	H (MPa)
Step 1		
P	6.31 ± 0.37^a	286.18 ± 16.97^A
P-CS _{15/500}	8.19 ± 0.35^b	381.89 ± 16.47^B
P-CS _{15/750}	7.88 ± 0.42^c	395.41 ± 25.22^C
Step 2		
P	6.91 ± 0.73^a	290.47 ± 29.69^A
P-CNC	7.73 ± 1.51^b	321.36 ± 43.26^B
P-CS ₂₀₃₄	7.33 ± 0.82^{ab}	353.50 ± 83.52^C

Results are expressed as mean values and standard deviation. Different superscripts within a group (i.e., within each parameter for each step) refer to a statistically significant difference ($p < 0.05$).

Graphical Abstract



ACCEPTED MANUSCRIPT

SCRIPT